

# Nanoscale

Accepted Manuscript



This is an *Accepted Manuscript*, which has been through the Royal Society of Chemistry peer review process and has been accepted for publication.

*Accepted Manuscripts* are published online shortly after acceptance, before technical editing, formatting and proof reading. Using this free service, authors can make their results available to the community, in citable form, before we publish the edited article. We will replace this *Accepted Manuscript* with the edited and formatted *Advance Article* as soon as it is available.

You can find more information about *Accepted Manuscripts* in the [Information for Authors](#).

Please note that technical editing may introduce minor changes to the text and/or graphics, which may alter content. The journal's standard [Terms & Conditions](#) and the [Ethical guidelines](#) still apply. In no event shall the Royal Society of Chemistry be held responsible for any errors or omissions in this *Accepted Manuscript* or any consequences arising from the use of any information it contains.

## ARTICLE

# Flexible 3D Porous CuO Nanowire Arrays for Enzymeless Glucose Sensing: *In Situ* Engineered versus *Ex Situ* Piled†

Cite this: DOI: 10.1039/x0xx00000x

Jianfei Huang, Yihua Zhu\*, Xiaoling Yang, Wei Chen, Ying Zhou and Chunzhong Li\*

Received 00th January 2012,  
Accepted 00th January 2012

DOI: 10.1039/x0xx00000x

[www.rsc.org/](http://www.rsc.org/)

Convenient determination of glucose in a sensitive, reliable and cost-effective way has aroused sustaining research passion, bringing along assiduous investigation for high-performance electroactive nanomaterials to build enzymeless sensors. In addition to the intrinsic electrocatalytic capability of the sensing materials, electrode architecture at microscale is also crucial for fully enhancing performance. In this work, free-standing porous CuO nanowire (NW) was taken as a model sensing material to illustrate this point, where *in situ* formed 3D CuO nanowire array (NWA) and CuO nanowires pile (NWP) immobilized with polymer binder by conventional drop-casting technique were both studied for enzymeless glucose sensing. The NWA electrode exhibited greatly promoted electrochemistry characterized by decreased overpotential for electro-oxidation of glucose and higher sensitivity over 5-fold of the NWP counterpart, beneficial from the binder-free nanoarray structure. Besides, its sensing performance was also satisfying in terms of rapidness, selectivity and durability. Further, the CuO NWA was utilized to fabricate a flexible sensor which showed excellent performance stability against mechanical bending. Thanks to its favorable electrode architecture, the CuO NWA is believed to offer opportunities for building high-efficiency flexible electrochemical devices.

## Introduction

Realizing sensitive, rapid and convenient detection of glucose is highly desirable for a range of occasions including fundamental biological research, bioengineering applications, food industries, and diagnosis/monitoring of diabetes, for which enzyme-involved biosensors have been extensively explored due to the highly selective bio-redox interaction between the enzymes and glucose.<sup>1,2</sup> Nevertheless, expensiveness, limited durability, critical operational conditions, complicated electrode construction and challenges in direct electron transfer have cast shadow on them.<sup>3,4</sup> In this context, passionate endeavor has been dedicated to exploring enzymeless electrochemical

platforms for glucose sensing.<sup>5,6</sup> Excellent in electrocatalysis as they are, noble metals and their alloys are not economical for large-scale manufacturing considering the prohibitive price and the scarcity of the raw materials. Vulnerability to chloride ion (Cl<sup>-</sup>) poisoning also has their utility seriously degraded.<sup>3,7,8</sup> Currently, non-precious transition metals and metal oxides are drawing increasing attention as cost-effective alternatives. Cupric oxide (CuO) was shown to be an attractive earth-abundant transition metal oxide for building enzymeless platforms for electrochemical detection.<sup>5,6,8,9</sup> In addition to rational selection of candidate electroactive materials, performance enhancement has also been enabled by downsizing the electrode materials. Fruitful results in electrochemical fields

including chemical sensing,<sup>10</sup> fuel cells,<sup>11</sup> (photo)electrochemical water splitting,<sup>12,13</sup> Li-ion batteries<sup>14</sup> and supercapacitors<sup>15</sup> have vividly instantiated promoted

electrode kinetics and performance upgrade attained by nanoscaling electrode materials that provide massively enlarged

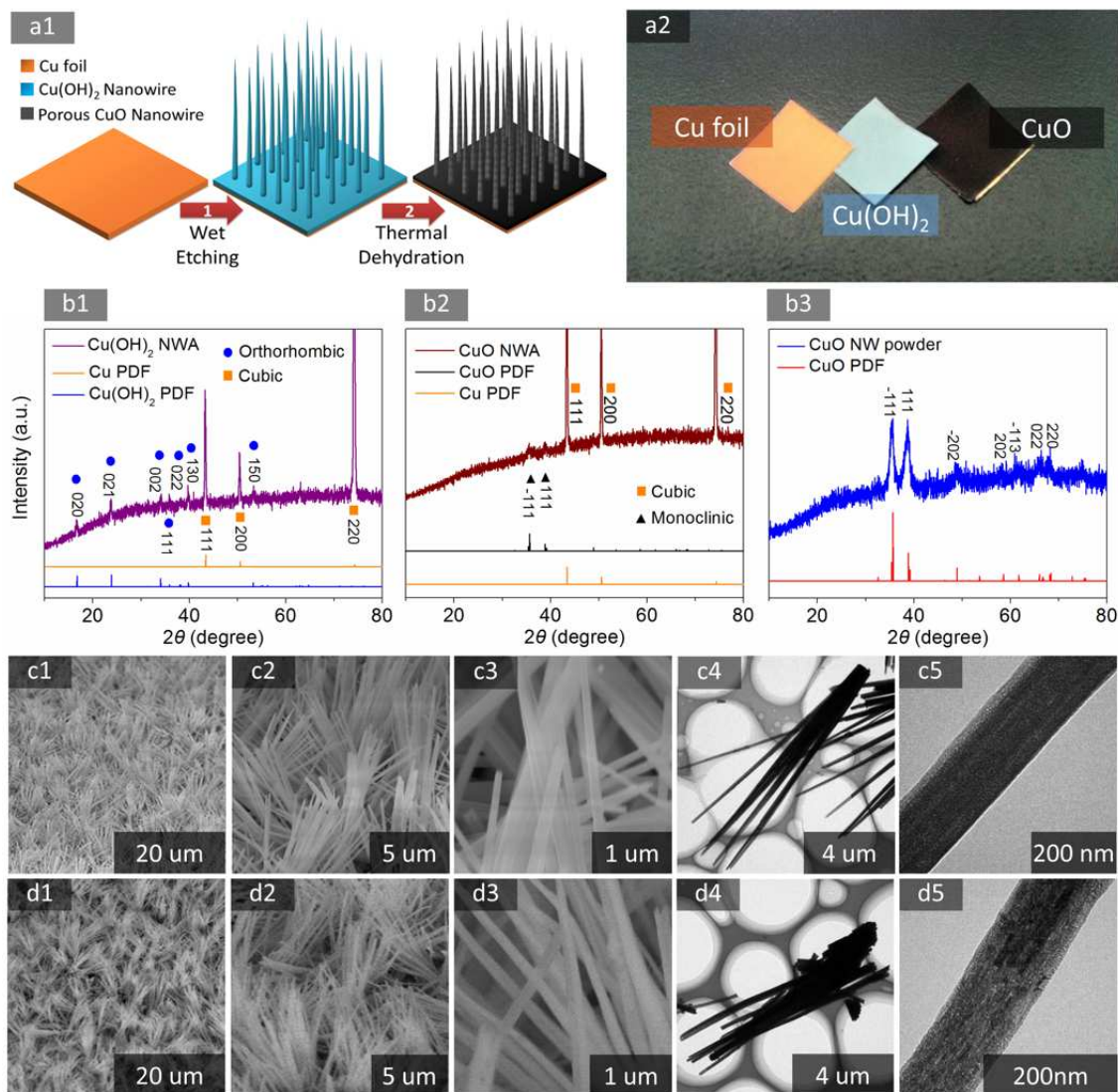


**Fig. 1** (a1) Schematic illustration of synthesis of porous CuO NWA on copper foils; (a2) digital photograph of a primitive Cu foil and the foils covered with Cu(OH)<sub>2</sub> and CuO NWA; XRD patterns of Cu(OH)<sub>2</sub> NWA (b1), CuO NWA (b2) and CuO NW powders (b3); SEM images of Cu(OH)<sub>2</sub> NWA (c1 to c3) and CuO NWA (d1 to d3); TEM images of Cu(OH)<sub>2</sub> NW (c4 to c5) and CuO (d4 to d5) NWs.

surface areas and mass transport resistance.<sup>16,17</sup> Particularly, one-dimensional (1D) nanostructures (wire, tube, rod and belt) incorporating defined charge transport pathways and abundant surface areas, have gained considerable research popularity in microelectronics and electrochemistry, holding exciting promise for building next generation of nanoelectronics and electrochemical devices.<sup>10,13-16,18-21</sup> In this work, we thereby sought to exploit 1D CuO NW as the electrode material for enzymeless glucose sensing.

Micro-/nano-scale morphologies of electrocatalysts have received huge attention as decisive factors of their performance.<sup>22,23</sup> However, less emphasis was given on the influence of electrode architecture at the level between nano-

sized electrocatalytic units and macroscopic electrodes, which calls for more attention if the electrocatalytic potential are to be fully realized. Consider the case of 1D nanomaterials, vertically aligned array structure<sup>10,16,24,25</sup> and disorderly piled-up nanowires<sup>26-29</sup> are the two most common electrode architectures for present amperometric sensors. An issue arising concerns for the latter is that it typically requires assistance of co-casted polymer binders such as Nafion, polyvinylidene fluoride (PVDF) or chitosan to form matrix film within which the active substances can be immobilized and connected to the current collector. Negative effects of employment of binders have been widely ascribed to the strong diffusion resistance and inevitable circumstance of partial blocking/burying of the electroactive

materials.<sup>16,30-32</sup> Moreover, the polymer binders usually make no contribution to catalysing the reactions themselves, have poor conductivity, and introduce additional costs and technical manipulations. To circumvent this, synthetic strategies as well as overall electrode design should be considered to realize *in situ* nanowire structure. Well-aligned vertical array of CuO NWs can be developed by hot plate method,<sup>33</sup> which was based on to fabricate functional electrodes.<sup>16,34,35</sup> Unfortunately, scaling-up of this method is hindered by the high temperature and long annealing duration required. It also often causes serious oxidation in thin foil substrate, which may suffer from deformation and embrittlement,<sup>16</sup> leaving it difficult for further device assembly. Therefore, it is necessary to design another route that avoids these unwanted consequences.

With the above motivations, we herein present the *in situ* synthesis of vertical porous CuO nanowire array (NWA) on conductive substrate via a conversion strategy. The as-prepared CuO NWA was then applied to enzymelessly detect glucose with high sensitivity, reliable stability and eligible selectivity, and its superiority over binder-coated CuO NWs modified electrode was studied. Furthermore, thanks to the moderate temperature in the preparation process, the thin foil as the supporting substrate of CuO NWA remained metallic without being totally oxidized into crispy copper oxides, allowing further integration with polyethylene terephthalate (PET) to obtain an archetypal flexible sensor that gave stable amperometric signal feedbacks under and after mechanical bending.

## Results and discussion

### Materials Synthesis and Characterizations

Ambient dry oxidation of copper substrates has been found to produce large-area vertical CuO NWs. Despite its one-step directness and facility over template-mediated methods, this approach requires a temperature up to 400-500 °C at least and relative long heating duration,<sup>33,34</sup> which is rather energy-intensive, time-consuming, and renders thin substrates mechanically fragile and poorly conductive. Hence, an alternative route towards high-density array of CuO NW was adopted in the present work, which utilized solution-processed Cu(OH)<sub>2</sub> NWA as the precursor.<sup>36</sup> The preparation route is illustrated in Fig. 1a1. A copper foil was subject to an alkaline oxidative etchant solution (AOES) containing (NH<sub>4</sub>)<sub>2</sub>S<sub>2</sub>O<sub>8</sub> and NaOH to generate Cu(OH)<sub>2</sub> NWA at room temperature, followed by thermal treatment at a much lower temperature (180 °C) for simultaneous dehydration of Cu(OH)<sub>2</sub> and improved crystallization of CuO,<sup>37</sup> giving the final product of CuO NWA. Successful realization of the synthetic route was initially indicated by the stepwise color changes of the starting foil from bright orange typical of metallic Cu to blue of the intermediate Cu(OH)<sub>2</sub> NWA and eventually dark brown of the target product CuO NWA, which are shown in Fig. 1a2. Moreover, it can be seen that the cut edge of the CuO NWA foil has metallic luster, visually suggesting limited oxidation into the thickness of the thin foil substrate.

Component identification was conducted using X-ray diffraction (XRD). The XRD patterns in Fig. 1b1 and Fig. 1b2 are for the foils covered with Cu(OH)<sub>2</sub> and CuO NWAs respectively. For the former, diffraction peaks at 16.6°, 23.7°, 34°, 35.8°, 38.1°, 39.7° and 53.3° are clearly discernible, corresponding well to (020), (021), (002), (111), (022), (130), (150) planes of orthorhombic structured Cu(OH)<sub>2</sub>. Note that the three strong diffraction peaks at 43.3°, 50.4° and 74.3° in correspondence to cubic structure of metallic copper are from the Cu substrate. However, the latter one only gives two faintly recognizable peaks at 35.5° and 38.8° characteristic of (-111) and (111) planes of the monoclinic CuO. This moderate signal is possibly due to the strong signals from the underlying Cu substrate and the small size of the CuO crystalline grain. Therefore, scratched CuO NW powders were also studied, whose XRD pattern is shown in Fig. 1b3. The powdery sample typically demonstrated improved diffraction peak signal, showing a series of diffraction peaks that confirm the existence of monoclinic crystalline CuO. Notably, for both foil samples, the existence of metallic Cu can be verified, again confirming limited thermal oxidation of the Cu substrate in our synthetic conditions, guaranteeing good conductivity and flexibility for subsequent usage. Also, no diffraction peaks can be attributed to Cu<sub>2</sub>O or Cu(OH)<sub>2</sub> for both the foil and powdery samples, determining the complete decomposition of Cu(OH)<sub>2</sub> and purity of CuO phase.

The microstructure of Cu(OH)<sub>2</sub> and CuO NWs were characterized by field-emission scanning electron microscopy (FE-SEM) and transmission electron microscopy (TEM) as shown in Fig. 1c and 1d, respectively. As can be seen in Fig. 1c1, the surface of the copper foil is covered with large-area grass-like Cu(OH)<sub>2</sub> NW with high density and good uniformity. These vertical nanowires are in a radially protruding fashion as shown in Fig. 1c2. The further magnified view in Fig. 1c3 shows axial straightness of the nanowires and the diameter is about 100-200 nm, with a tapering outline. Interestingly, the CuO NWs are arranged in a manner that several closely aligned nanowires share a common bundled end. This is further ascertained by TEM characterization shown in Fig. 1c4. In accordance to the SEM characterization, the closely grown Cu(OH)<sub>2</sub> NWs have common connection at their 'roots', which was so firm that remained undamaged after ultrasonication during of TEM sample preparation. The nanowires are about 10 um in length, which can also be estimated in the SEM images. Fig. 1c5 offers a close-up view of a single Cu(OH)<sub>2</sub> NW. The surface of the nanowire is generally smooth with a slightly discernible sign of the existence of porous outer shell, possibly owing to the instability of Cu(OH)<sub>2</sub> under the high-energy electron beam impact in TEM characterization, which leads to partial decomposition.<sup>38</sup> All these results demonstrate the successful *in situ* preparation of vertical Cu(OH)<sub>2</sub> NWA using the mild wet chemical etching protocol. This method towards aligned NWA requires no templates,<sup>25,39</sup> shape-directing agent,<sup>40</sup> noble metal intermediates<sup>41</sup> or pre-seeding on substrates,<sup>13,42</sup> making it a facile choice potentially promising for scaled-up production. Moreover, acid-removable nature of Cu(OH)<sub>2</sub> implies this protocol can be possibly extended to synthesize other functional NWA structure with the Cu(OH)<sub>2</sub>



NWA as sacrificial template.<sup>18</sup> The formation of  $\text{Cu}(\text{OH})_2$  NWA was resulted from interaction between the Cu species and etchant in the AOES. Specifically, as the oxidative  $\text{S}_2\text{O}_8^{2-}$  attacks Cu at the foil surface,  $\text{Cu}^{(0)}$  is oxidized to  $\text{Cu}^{(\text{II})}$  and

dissolved as ion into the solution. Instead of diffusing away,  $\text{Cu}^{(\text{II})}$  interacts with  $\text{OH}^-$  and construct themselves in a manner similar to self-assembly. The high pH (>14) milieu

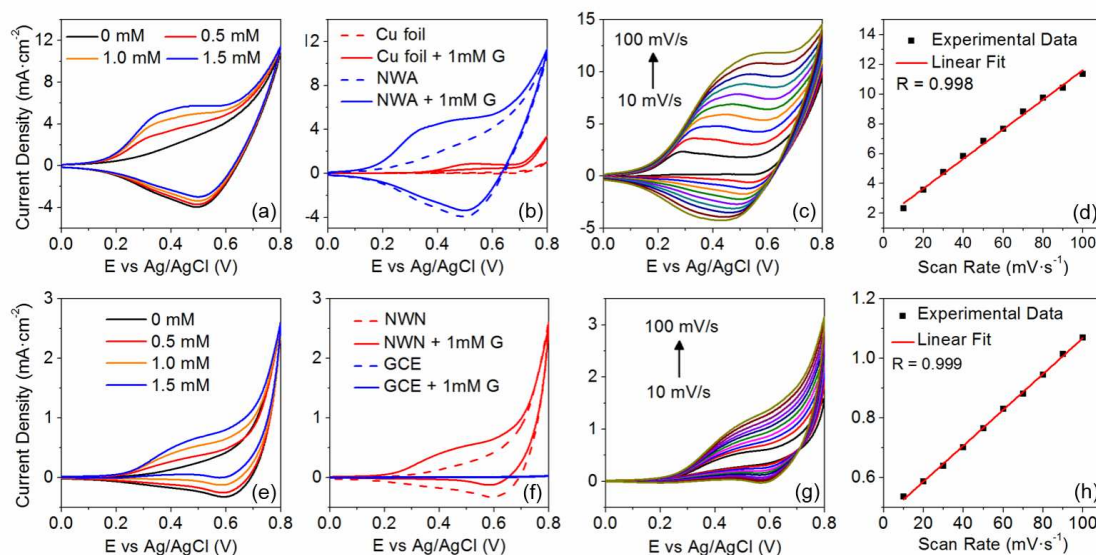


**Fig. 2** CV profiles with different concentrations of glucose of (a) CuO NWA and (e) CuO NWP; CV with glucose in absence and presence for (b) CuO NWA compared with planar Cu electrode and (f) CuO NWP compared with GCE; CV at scan rates from 10 to 100  $\text{mV}\cdot\text{s}^{-1}$  for (c) CuO NWA and (g) CuO NWP in 2.5 mM glucose. (d) The calibration plot of (c); (h) The calibration plot of (g).

subsequently leads to evolution of corrugated layers of  $\text{Cu}(\text{OH})_2$ , which grows by oxidation reaction of  $\text{Cu}^{2+}$  and  $\text{OH}^-$  preferentially along the [100] direction because of the shortest inter-planar distance of (100) and the relatively stronger hydrogen bonding interaction.<sup>36</sup> In this dissolution and bottom-up way, the one-dimensional morphology is thus formed.

Successful transformation from  $\text{Cu}(\text{OH})_2$  to CuO is unambiguously demonstrated in the XRD patterns as was discussed. The SEM images in Fig. 1d1 to 1d3 present the as-prepared CuO NWA at various magnifications, from which no significant variance of the NWA morphology is observed. This is possibly due to the controlled heating rate in the annealing procedure that prevented fierce  $\text{H}_2\text{O}$  vapor departure in the dehydration reaction, which may threaten to cause rupture of the nanowires. Fig. 1d4 presents a TEM image of the CuO NWs, where it is found that the nanowires are slightly shorter than their  $\text{Cu}(\text{OH})_2$  precursor. In addition, as we observed the sample using TEM, we found more small broken pieces of nanowire in the case of CuO than that of  $\text{Cu}(\text{OH})_2$ , which suggested intensified breakage of the CuO NWs during ultrasonication for sample preparation. A close-up examination of a CuO NW is presented in Fig. 1d5. Compared to the  $\text{Cu}(\text{OH})_2$  NW in Fig. 1c5, porosity in CuO NW is more evident, which is perceptible not only at the outer shell. Further magnified TEM images in Fig. S1 reveals that CuO NW is composed of closely interconnected small CuO particles with pores and gaps in between. The porous structure was further characterized by nitrogen sorption isotherms that present typical type-IV isotherms and the pore size distribution

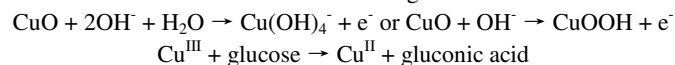
determined from the adsorption branch with the Barrett-Joyner-Halenda (BJH) method are shown in Fig. S3. Apparently, dehydration reaction caused breakage of the  $\text{Cu}(\text{OH})_2$  NW bulk into smaller CuO particles that remained in touch with each other and preserved the overall 1D morphology. This should answer for the aggravated susceptibility to ultrasonication since the CuO NWs with increased porosity have weakened mechanical strength along its high aspect-ratio axial direction compared to the  $\text{Cu}(\text{OH})_2$  counterpart. Despite this, the porous profile which provides further increased surface area may be favorable for electrochemical sensing application. Understandably, the porosity evolved during dehydration where  $\text{H}_2\text{O}$  vapor evaporated out and left pores in the nanowire bulk. This mechanism of generation of pores, which is unique from those reported protocols engaging sacrificial templates,<sup>43</sup> pore-forming agents,<sup>44</sup> and electrochemical ion insertion,<sup>45</sup> possibly offers a general and facile approach for porous metal oxide nanostructures from the corresponding hydroxide precursors to be further explored.

### Enzymeless sensing of glucose

Efficient utilization of nano-sized electrocatalysts as building blocks to construct high-performance sensor electrodes remains to be challenging. Electrode construction techniques and electrode architectures of catalytic materials can exert considerable influence on the performance. Herein, with the *in situ* prepared CuO NWA, we carried out proof-of-concept research to study the performance of the two most representative nanowire architectures for amperometric sensing of glucose.

Firstly, two types of electrodes were prepared. One featured electrode architecture of vertical nanowire array (denoted as NWA) while the other was fabricated by conventional modification protocol, with CuO NWs piled (denoted as NWP) randomly in Nafion film that was drop casted on a glassy carbon electrode (GCE). Its microscopic image was shown in Fig. S2, while the microstructure of the working portion of the NWA electrode is considered the same as the freshly prepared samples. For both electrodes, the weight of the CuO NW per geometric surface area ( $W_{\text{CuO}}/S_{\text{(geo)}}$ ) was kept identical. The details and fabrication flowchart (Fig. S3) can be found in the experimental section and Electronic Supporting Information (ESI), respectively. To collect information of the electrocatalytic ability of the CuO NW-based electrodes towards glucose electro-oxidation, evaluation by means of cyclic voltammetry (CV) was first performed (Fig. 2). For the NWA electrode, when glucose is can be observed in the positive scan from 0 V to 0.8 V (Fig. 2a). With increased concentration of glucose, an oxidation peak around 0.35 V appeared. For the reverse scan from 0.8 V to 0 V, the cathodic current experienced gradual decrease as glucose concentration increased. These observations typically indicated an irreversible electro-oxidation process of glucose. In Fig. 2b, the CV curves of a primitive planar Cu electrode (PCE) is presented in comparison with the CuO NWA. Clearly seen, the PCE can also electro-oxidize glucose, with increased anodic current peaking at 0.51 V and the turn-on potential is situated at around 0.36 V. Both positively shifted potential parameters suggest the sluggish electro-oxidation kinetics of the PCE compared to the CuO NWA, whose turn-on potential was as low as 0.18 V. Peaking current density is also far higher for the NWA. Facilitated electrocatalytic oxidation of glucose from the CuO NWA is unequivocally derived from the cooperative effect of the electroactive CuO and nanoengineered NWA structure. Also, it is noted for the blank sample (without glucose), the CuO NWA exhibits much higher current density than the primitive Cu foil planar electrode, suggesting significantly increased surface area, surface energy and boosted electron transfer from the vertically protruding porous CuO NWs.<sup>8</sup> The CV data of the CuO NWP electrode was also recorded. It is not surprising that the NWP electrode was able to carry out the irreversible electro-oxidation process (Fig. 2e) analogous to the NWA one. Since there is no signal typically corresponds to electro-oxidation of glucose at a bare GCE (Fig. 2f), the electrocatalytic effect of the NWP electrode is undoubtedly attributed to the CuO NWs. Notably, *ex situ* introduction of CuO NWs also leads to significantly amplified background current compared to the bare GCE, which exemplifies the advantage of nanostructured electrodes in enhancing electrode-electrolyte interactions. All these taken into account, the feasibility of using the as-prepared CuO NW for enzymeless glucose sensing is preliminarily confirmed. The electro-oxidation process at the two electrodes was further explored by CV at different scan rates ranging from 10-100 mV·s<sup>-1</sup>, as shown in Fig. 2c and 2g, and the relationship linearly fitted in Fig. 2d and Fig. 2h suggests the surface adsorption-controlled nature of the electrocatalytic process.

While the explicit mechanism for CuO-catalyzed electro-oxidation of glucose in alkaline has not been completely settled, generally accepted proposal suggests formation of high valence Cu<sup>III</sup> intermediate that readily oxidizes glucose into gluconic acid,<sup>3,5</sup> which can be described with the following reactions:



Accordingly, the mechanism for electrochemical sensing of glucose by the NWA and NWP electrodes is depicted in Fig. 3. Cu<sup>II</sup> is electro-oxidized to Cu<sup>III</sup>, which is a highly oxidative species and subsequently interacts the adsorbed glucose at the nanowire surface, oxidizes it into gluconic acid and gets itself reduced to the original Cu<sup>II</sup>. Upon this cycling, electrons generated from the electro-oxidation of Cu<sup>II</sup> transport through the nanowire to the underlying conductive substrate, generating anodic signal.

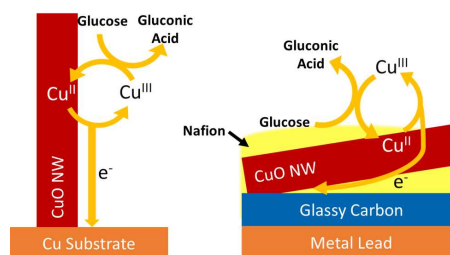


Fig. 3 Mechanism of the electro-oxidation of glucose at the CuO NW-based electrodes

Amperometric *i-t* analysis was carried out to deduce the linear relationship between the analyte concentration and current responses of the NWA and NWP electrodes, with their respective peaking potentials applied during the tests. Generally, both of them give stair-like *i-t* curves under stepwise addition of glucose, with the low-concentration parts magnified in the respective insets, as shown in Fig. 4a and 4b. Upon the test, after the current reached a steady state, a predetermined amount of glucose was successively injected into the magnetically-stirred solution, which immediately induced leaping of the current. Rapidness of signal response of the CuO NWA was confirmed by observation of the magnified amperometric curves (Fig. S4), which show 90% current change was completed in about 1 s and current plateaus were generally achieved in 2 s within the linear range. This fast current response is benefited from the high surface area 1D morphology and the open spaces in the nanowire array structure that allow adequate interfacing with the solution phase and facilitated diffusion of analyte molecules. The NWP also offered comparably quick current feedback. When the analyte concentration reached a certain level, amperometric signal became saturated. The concentration-signal relationship is plotted in Fig. 4c. Note that for comparison, *i-t* performance of the NWP electrode under 0.35 V (the working potential used for the NWA electrode) was also recorded (Fig. S5). The calibration equations deduced from linear regression of the experimental data for the NWA (1), NWP under 0.45 V (2) and 0.35 V (3) are listed as below:

$$J (\text{mA} \cdot \text{cm}^{-2}) = 1.42034 C (\text{mM}) + 0.11254 \quad (1)$$

$$J \text{ (mA}\cdot\text{cm}^{-2}) = 0.25012 C \text{ (mM)} + 0.01707 \quad (2)$$

$$J \text{ (mA}\cdot\text{cm}^{-2}) = 0.19712 C \text{ (mM)} + 0.00359 \quad (3)$$

where  $J$  and  $C$  stand for current density and analyte concentration, respectively. As fitted, the CuO NWA demonstrated an excellent

is 7 times that of the NWP. When the working potential was optimized at the respective peaking potentials, the NWA still shows a sensitivity above 5 times higher than the NWP despite working at a lower (by 100 mV) potential. In addition to its outperforming performance over the NWP electrode in this work, the overpotential for the CuO NWA to carry out sensing functionality is also smaller than most CuO-based glucose sensors,<sup>8,17,46-50</sup> and the sensitivity exceeds many *ex situ* immobilized 1D CuO-based enzymeless glucose sensors, as listed for comparison in Table S1.

While the NWA and NWP electrodes both have shown improved electrochemistry compared with the primitive PCE and bare GCE, the former obviously overshadowed the latter. As the apparent  $W_{\text{(CuO)}}/A_{\text{(geo)}}$  of electrocatalyst was pre-controlled, possibility of the amount of active material as a main cause of performance difference can be ruled out. The positive sweeping of the CV of the electrocatalytic reaction on which the sensing functionality is based has been studied, as shown in Fig. 5a. In addition to the aforementioned higher anodic peak potential (by ~100 mV) of the NWP, the reaction turn-on potential of the NWP (0.23 V) is also positively shifted by about 50 mV compared with the NWA. Obviously a higher overpotential is required for the NWP. Also, the current magnitude of the NWA is also much larger than the NWP. We first sought to consider these phenomena from the view of activity degradation of CuO in the NWP electrode. Actually, this is hardly possible because the sensor fabrication procedures induced no force powerful enough to chemically change the stable CuO. Besides, the Tafel plot in Fig. 5b also reveals that the NWA and NWP have very close Tafel slopes, 163 mV·dec<sup>-1</sup> for the NWP and 169 mV·dec<sup>-1</sup> for the NWA. Since the Tafel slope is related to the activation energy of a certain electrochemical reaction, this denies change of catalytic ability as a determining factor that brought about the varied performances.

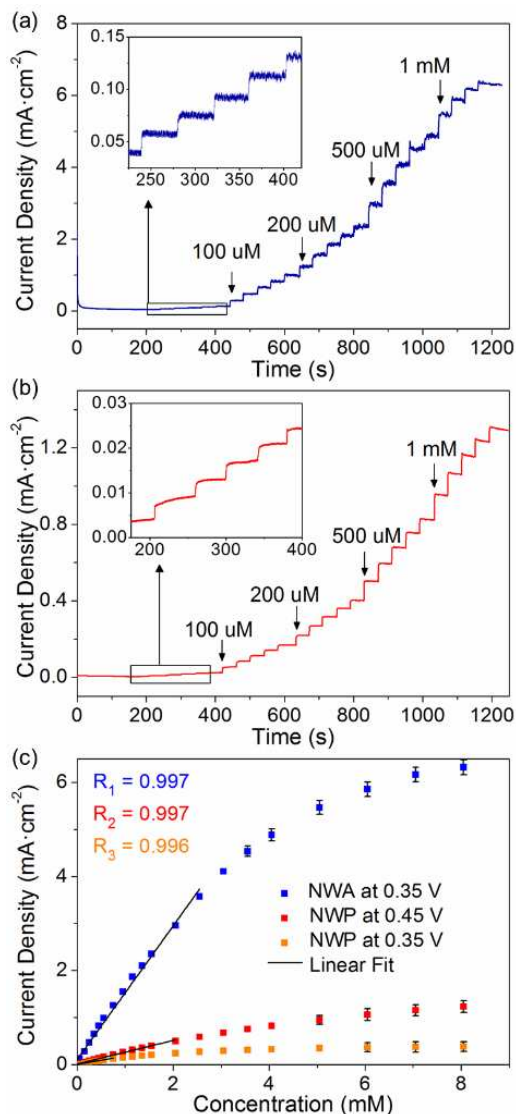


**Fig. 4** Amperometric  $i$ -t test with successive addition of glucose for the NWA under +0.35 V (a) and the NWP under +0.45 V; (c) calibration plots of (a) and (b). The insets show respective  $i$ -t curves at low concentration levels, with stepwise addition of 10  $\mu$ M glucose.

sensitivity of 1420.3  $\mu\text{A}\cdot\text{cm}^{-2}\cdot\text{mM}^{-1}$  with a linear range up to ~2.55 mM and a detection limit of 5.1  $\mu\text{M}$  (3 signal-noise ratio). The CuO NWP exhibited a sensitivity of 250.1  $\mu\text{A}\cdot\text{cm}^{-2}\cdot\text{mM}^{-1}$ , a linear range up to ~2.05 mM and a detection limit of 1.9  $\mu\text{M}$ , under the applied potential of 0.45 V. For its counterpart under 0.35 V, the corresponding performance parameters are determined to be 197.1  $\mu\text{A}\cdot\text{cm}^{-2}\cdot\text{mM}^{-1}$  (sensitivity), ~0.75 mM (linear range) and 0.7  $\mu\text{M}$  (detection limit). Obviously, among the three cases, the NWA presents a much higher sensitivity than the other two. When the applied potential was the same (0.35 V), the sensitivity of the NWA

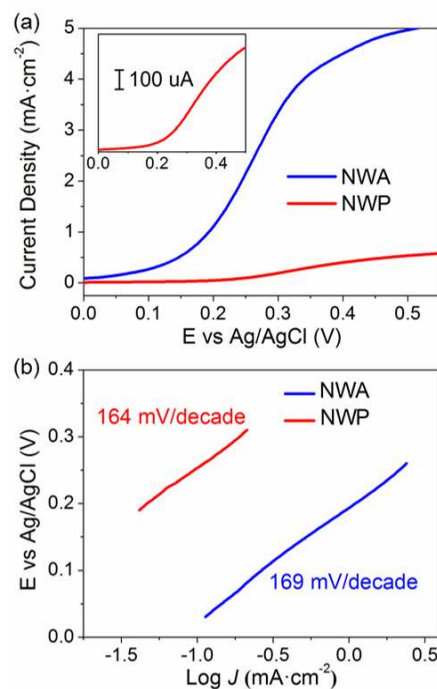




Fig. 5 (a) positive scanning of CV measurements with 1 mM glucose in presence, inset shows the magnified curve for the NWP; (b) the corresponding Tafel plot of (a).

Therefore, the performance difference must be connected to the overall electrode architecture. Due to the inherent structure

of the modifying film in the NWP electrode, disorderly stacking style can result in a portion of nanowires that failed to gain

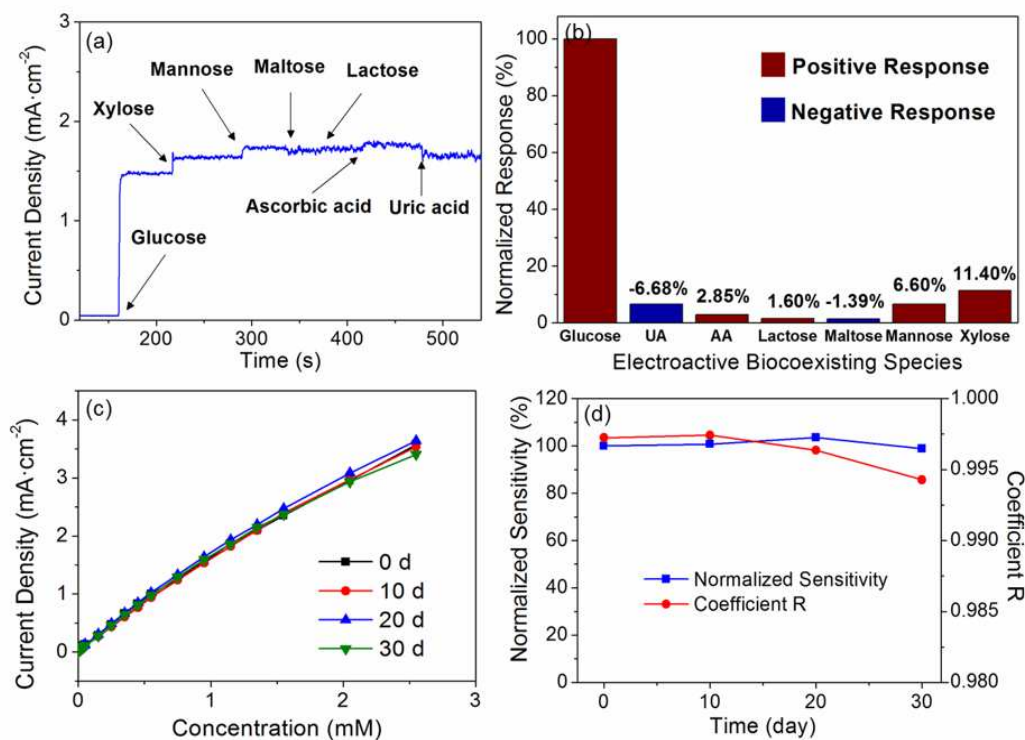


Fig. 6 (a) Amperometric test for selectivity and anti-Cl<sup>-</sup>-poisoning of the NWA sensor and (b) percentage of interfering signals to the target analyte. (c) Calibration plots within the linear range and (d) normalized sensitivity and the corresponding Pearson coefficients of the CuO NWA sensor after different days.

direct contact to the conductive GC, which resembles a film of stacking nanoparticles where defined charge transport pathway is absent and electrons have to go through multiple interfaces. Both aspects weaken the positive effect of CuO NWs in shuttling electrons between the analyte and the current collector. As a consequence of the increased interfacial resistance, the overall series resistance becomes larger, which can be determined using electrochemical impedance spectroscopy (EIS). Both the NWA and NWP electrodes feature a reaction-controlled part (semicircle) at frequencies and a diffusion-controlled part (oblique line) at low frequencies in their Nyquist plots (Fig. S6). As the diameter of the semicircle reflects the electron

transfer resistance,  $R_{et}$ , it can be found  $R_{et}$  of the NWA is much smaller compared to the NWP electrode, in accordance with the performance and analysis, implying better electron transfer.<sup>51,52</sup> Also, as we characterized CuO NWP-Nafion film (Fig. S7), it is found isolation of fractured CuO NWs may occur, namely nano-sized CuO was isolated within/on the polymer matrix without contact with other CuO NWs or the conducting GC. This can be aggravated when the ultrasonication, although important for forming homogeneous casting suspension, led to more low-aspect-ratio CuO particles from the mechanical fracture of the CuO NWs. Such isolated CuO and those blocked by Nafion polymer binder, cannot engage in

electrocatalysis by failing as electrochemically active bridge between the analyte and the GC. In contrast, both good electron transport between the catalytic units and the external circuit, and abundance of electrochemically connected and analyte-accessible active sites exist in the NWA electrode, which favors the sensing platform to make full use of the active CuO.

In further exploring the CuO NWA for as a reliable platform for enzymeless glucose sensing, practical testing conditions need be taken into consideration. In real samples, co-existing electroactive species with comparable reducibility such as ascorbic acid (AA), uric acid (UA) and other reducing sugars with similar chemical structures may cause unwanted interference. The relative high concentration (~100 mM) of Cl<sup>-</sup> in blood, which was reported to poison some metal-based sensors, must also be concerned. To find out whether the selectivity of the sensor is good enough to preclude interference from the mentioned species and its poisoning-proof ability against Cl<sup>-</sup>, we further conducted amperometric *i-t* test with different interfering species successively added and the supporting electrolyte containing 0.2 M NaCl. The concentration of the interfering species was fixed 1/10 of the glucose despite their actually lower ratio (1/40 to 1/30) to glucose in human blood.<sup>53</sup> As shown in Fig. 6a, the steady current experienced significant increase as 1 mM glucose was added at the experimental runtime of 160 s. In contrast, only moderate current responses can be observed when the



interfering species including xylose, mannose, maltose, lactose, AA and UA were successively added. Interfering signals were -6.68%, 2.85%, 1.60%, -1.39%, 6.60% and 11.40% for the respective species (Fig. 6b), which were all acceptable. What's more, despite the high concentration of  $\text{Cl}^-$  in presence, the sensor's response was not degraded. Further recovery test was performed to demonstrate its reliability (Fig. S9), where blood glucose mimic liquid (LifeScan, Inc.) with pre-determined concentration was injected twice into the electrolyte followed by two-time injection of 20  $\mu\text{M}$  standard concentration of glucose. The results of the recovery test tabulated in Table S2 shows the respective recovery of 95% and 98%, and the relative deviation of the found concentrations for blood glucose mimic liquid from the commercially calibrated value is less than 6%. The long-run stability of the CuO NWA sensor was also evaluated by testing its performance after having left the NWA electrode in ambient condition without special protection for 10, 20 and 30 days. The absolute current responses (Fig. 6c) showed no dramatic change. Besides, the sensitivity and linear relevancy (Fig. 6d) neither experienced great variance. A slight decrease of sensitivity by less than 2% over a period of 30 days is much lower than the data reported in a series of literature on enzymeless glucose sensors.<sup>49-51,54,55</sup> This splendid retention of sensitivity could be attributed to the synergistic effect of the stable chemical property of CuO and the exceptional flake-off resistance of the *in situ* grown NWA structure.

#### Flexible CuO NWA as bendable sensor electrode

The advantage of *in situ* grown NWA on thin conductive substrate comes not only from the superior performance demonstrated above, but also from its compatibility to further integration into flexible devices. In Fig. 7a, small foil slice of CuO NWA is shown to be directly bent by hand. Endowing flexibility to electrodes is gaining growing preference due to the light-weight, durability, user-convenience, and feasibility for rolled-up production therefore acquired.<sup>56</sup> Consequently, an archetypal flexible sensor (Fig. 7b) was constructed. Reliability of the sensing performance against mechanical input was assessed by amperometry. First, the exposed area ( $3.5\text{ cm} \times 0.6\text{ cm}$ ) with CuO NWA was bent with the curvature radii ( $\rho$ ) fixated at 18.5 and 11.5 mm (Fig. 7c) and the  $i$ - $t$  responses to analyte addition were shown in Fig. 7e. At the moderate curvature ( $1/\rho = 0.0541\text{ mm}^{-1}$ ,  $\rho = 18.5\text{ mm}$ ), the current response towards 10, 50 and 100  $\mu\text{M}$  glucose showed negligible deviation from what was measured at the unbent condition ( $1/\rho = 0$ ,  $\rho = \infty$ ). Even when it reached a high curvature ( $1/\rho = 0.0870\text{ mm}^{-1}$ ,  $\rho = 11.5\text{ mm}$ ), the sensitivity remained 90% relative to the flat state. This proves the sensor has eligible performance stability against bending. To further explore its capability against mechanical fatigue, the sensor was mounted onto a home-made tester and the CuO NWA portion was repeatedly bent and relaxed. Fig. 7d displays the sensor under flat (upper) and maximum bending (lower) conditions. The CuO NWA portion got bent as the clamp moved left. After the maximum travel distance of 10 mm was completed, the clamp moved right until the bent CuO NWA returned to its original state. This bending-relaxation process made up one cycle. After 10, 100, and 1000 cycles, respective amperometric tests were performed. The current

curves in Fig. 7f clearly demonstrate the sensor exhibit robust performance reliability against long-run mechanical input, with insignificant departure from the flat condition after 1000 cycles. Although discernible response degradation was observed after 1000 cycles, performance conservation as high as 90% of the initial amperometric response was quite satisfying. These results indicate that the flexible CuO NWA has promise to be further engineered and optimized to construct flexible sensing devices with high sensitivity,

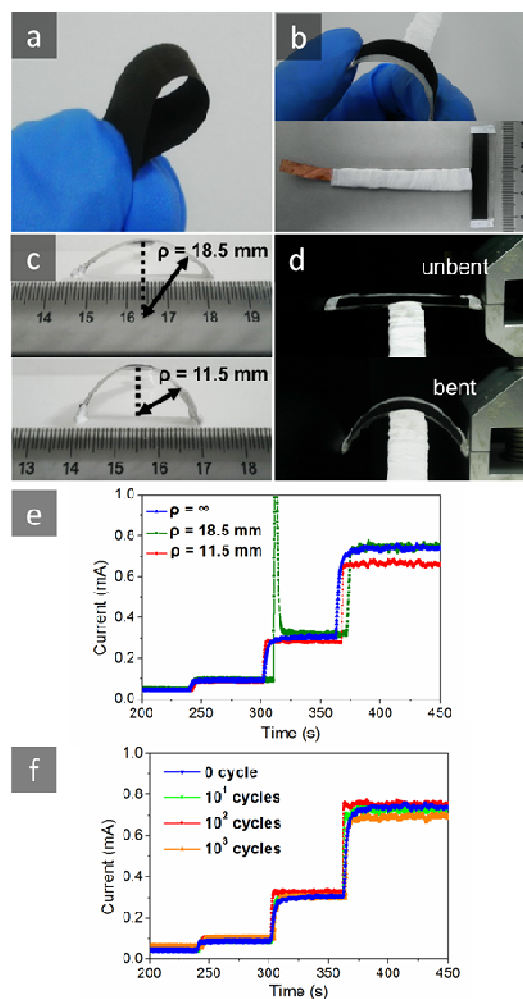


**Fig. 7** (a) A flexible slice of CuO NWA; (b) flexible sensor under its bent (upper) and unbent (lower) conditions; (c) flexible sensor bent with curvature radii of 18.5 mm (upper) and 11.5 mm (lower); and (d) bending-relaxation tests showing the sensor unbent (upper) and maximum bent (lower). Current response at different curvature radii (e) and after different bending-relaxation cycles (f) to addition of 10, 50 and 100  $\mu\text{M}$  glucose.

rapid response and robust durability.

#### Experimental

##### Synthesis of CuO NWA

The synthetic procedure involved solution-processed etching of copper foils and dehydration of the thus-obtained  $\text{Cu}(\text{OH})_2$  NWA. Typically, AOES was prepared by dissolving 0.913 g  $(\text{NH}_4)_2\text{S}_2\text{O}_8$  in 22 mL deionized water and dropwise addition of 8 mL freshly

prepared 10 M NaOH into the  $(\text{NH}_4)_2\text{S}_2\text{O}_8$  solution under moderate stirring. After the AOES cooled to room temperature, its pH ( $>14$ ) was confirmed. Cleaned with diluted HCl and successively ultrasonicated in acetone and ethanol, the copper foils (X%) were rinsed using deionized water and immediately immersed in the AOES. When the surface of the copper foils turned light blue, they were taken out of the solution, thoroughly rinsed with deionized water and dried in air. Then the samples went through four-hour dehydration under  $180^\circ\text{C}$  in air at a ramp rate of  $2^\circ\text{C}\cdot\text{min}^{-1}$ , whose color eventually turned to dark brown. The temperature was allowed to cool to room temperature gradually before opening the furnace.

### Sensor fabrication

For the NWA electrode, preparation of CuO NWA on a copper foil was the same as formerly described except that the degreased copper foil may be pre-masked by a piece of scotch tape before being dipped in the AOES. Subsequently, the CuO NWA was mounted on a plastic substrate with its rear side and the bare copper part (acting as the lead) sealed by thermosetting insulating epoxy. For the CuO NWP electrode, the CuO NWs were carefully collected using doctor-blade method and were dispersed in deionized water containing 0.5 wt% Nafion (Dupont). The concentration of the CuO NW were adjusted by the amount of the added solvent so that every 10  $\mu\text{L}$  of the suspension has the weight of CuO NW equivalent to the amount collected from 0.0707  $\text{cm}^2$  (the geometric surface area of the GCE, 3 mm in diameter) CuO NWA foil. After a GCE was successively polished with alumina powders (1 and 0.05  $\mu\text{m}$ ), 10  $\mu\text{L}$  of the suspension was drop-casted on the GCE, which was left to dry up naturally. For the archetypal flexible CuO NWA sensor, the starting copper foil was clipped into a desired shape for convenience in subsequent experiments. After the preparation of CuO NWA on the foil, the CuO NWA foil was firmly bound onto a tailored PET slice using soft double-sided adhesive tape, and the both ends were further secured by Teflon tape. The pre-masked metallic copper area for external electrical connection was sealed off from contact of electrolyte with epoxy resin and Teflon tape. The whole sensor electrode is T-shaped (Fig. 7b). Note that this shape was intentionally designed for facile operation of bending the CuO NWA part and can be further adjusted according to practical requirement.

### Characterization

X-Ray Diffraction (XRD) characterization (40 kV, 100 mA) was performed on an X-ray diffractometer (D/MAX 2550, Rigaku) equipped with a RINT2000 vertical goniometer and a Cu K $\alpha$  radiation generator. Microscopic analysis of foil samples and drop-casted CuO NW-Nafion film was carried out using field-emission scanning electron microscopy (FE-SEM, S-4800, Hitachi) at an accelerating voltage of 15.0 kV and emission current of 10  $\mu\text{A}$ . Micrographs of scratched nanowires were taken using transmission electron microscopy (TEM, JEM 2011, JEOL). Electrochemical measurements including cyclic voltammetry (CV), amperometric *i*-t tests and electrochemical impedance spectroscopy (EIS) were carried out with an electrochemical workstation (CHI660c, Shanghai Chenhua Co.) under conventional three-electrode configuration, employing a Pt wire electrode, an Ag/AgCl electrode (KCl-saturated) as counter electrode and reference electrode, respectively.

Working electrodes were different CuO NW-based electrodes or GCE electrodes modified with or without Nafion. 0.1 M NaOH supporting electrolyte and all standard analyte solutions were freshly prepared for all experiments. For all CV measurements, the scan rate is  $50\text{ mV}\cdot\text{s}^{-1}$  unless otherwise mentioned. Amperometric *i*-t data were collected under fixed potential and magnetically stirred condition. The standard analyte solution was injected after current curve reached a steady baseline. EIS was performed at a frequency range of 10k Hz to 0.01 Hz with amplitude of 5 mV employing 5 mM  $[\text{Fe}(\text{CN})_6]^{3/4-}$  in 0.1 M KCl as the redox probe.

### Conclusions

*In situ* synthesis of CuO NWA on conductive substrate has been realized and XRD, SEM and TEM were applied to confirm its structure and component. In addition to the extraordinary sensitivity and stability for enzymeless sensing functionality, with the *in situ* formed 3D array structure and intact connection to the underlying conducting substrate, the CuO NWA showed obviously enhanced electrode kinetics for glucose electro-oxidation and outperforming sensitivity over its counterpart of freely stacked CuO NWP entrapped within the polymer binder prepared by conventional casting, which suggests that the large-scale arrangement of nanowire electrocatalyst and the electrode architecture are crucial to efficient realize the sensing functionality of electroactive CuO NWs. The CuO NWA also showed compatibility to construction of a flexible sensing platform, which can give satisfyingly stable performance under and after mechanical bending. Beneficial from its *in situ* growth style and high-density vertical structure, as well as multifunctionality offered, by CuO, it can be inferred that the CuO NWA may become a useful tool for determining other bio-analytes, and can also be a potential candidate in other electrochemical applications, such as energy storage and conversion, etc.

### Acknowledgements

This work was supported by the National Natural Science Foundation of China (21471056, 21236003, 21206042, and 21176083), the Basic Research Program of Shanghai (13NM1400700, 13NM1400701), and the Fundamental Research Funds for the Central Universities.

### Notes and references

Key Laboratory for Ultrafine Materials of Ministry of Education, School of Materials Science and Engineering, East China University of Science and Technology, Shanghai 200237, China. Fax: +86 21 6425 0624; Tel: +86 21 6425 2022; E-mail: yhzhu@ecust.edu.cn (Y. Zhu); czli@ecust.edu.cn (C. Li).

† Electronic Supplementary Information (ESI) available: TEM images of CuO nanowires. SEM images of the composite film of CuO NWs in the Nafion binder. Flowchart of electrodes fabrication procedures. Current response time to addition of the glucose. Amperometric *i*-t test for the NWP under +0.35 V. Nyquist plot of the electrodes. SEM images of fractured parts of CuO nanowires at the NWP-Nafion film. Parameter

comparison of enzymeless sensors for glucose detection. See DOI: 10.1039/b000000x/

- 1 A. Heller and B. Feldman, *Chem. Rev.*, 2008, **108**, 2482.
- 2 J. Wang, *Chem. Rev.*, 2008, **108**, 814.
- 3 S. K. Meher and G. R. Rao, *Nanoscale*, 2013, **5**, 2089.
- 4 C. Chen, Q. Xie, D. Yang, H. Xiao, Y. Fu, Y. Tan and S. Yao, *RSC Adv.*, 2013, **3**, 4473.
- 5 G. Wang, X. He, L. Wang, A. Gu, Y. Huang, B. Fang, B. Geng and X. Zhang, *Microchim. Acta*, 2013, **180**, 161.
- 6 S. Park, H. Boo and T. D. Chung, *Anal. Chim. Acta*, 2006, **556**, 46.
- 7 J. Chen, W. D. Zhang and J. S. Ye, *Electrochem. Commun.*, 2008, **10**, 1268.
- 8 E. Reitz, W. Jia, M. Gentile, Y. Wang and Y. Lei, *Electroanalysis* 2008, **20**, 2482.
- 9 J. Huang, Y. Zhu, H. Zhong, X. Yang and C. Li, *ACS Appl. Mater. Interfaces*, 2014, **6**, 7055.
- 10 S. Su, X. Wei, Y. Guo, Y. Zhong, Y. Su, Q. Huang, C. Fan, and Y. He, *Part. Part. Syst. Charact.*, 2013, **30**, 326.
- 11 C.-J. Zhong, J. Luo, P. N. Njoki, D. Mott, B. Wanjala, R. Loukrakpam, S. Lim, L. Wang, B. Fang and Z. Xu, *Energy Environ. Sci.*, 2008, **1**, 454.
- 12 H. Tüysüz, Y. J. Hwang, S. B. Khan, A. M. Asiri and P. Yang, *Nano Res.*, 2013, **6**, 47.
- 13 Z. Yin, Z. Wang, Y. Du, X. Qi, Y. Huang, C. Xue and H. Zhang, *Adv. Mater.*, 2012, **24**, 5374.
- 14 B. Liu, X. Wang, H. Chen, Z. Wang, D. Chen, Y. B. Cheng, C. Zhou and G. Shen, *Sci. Rep.*, 2013, DOI:10.1038/srep01622.
- 15 X. Zhang, W. Shi, J. Zhu, D. J. Kharistal, W. Zhao, B. S. Lalia, H. H. Hng and Q. Yan, *ACS Nano*, 2011, **5**, 2013.
- 16 W. Jia, M. Guo, Z. Zheng, T. Yu, Y. Wang, E. G. Rodriguez and Y. Lei, *Electroanalysis*, 2008, **20**, 2153.
- 17 H. Wu, S. Zhou, Y. Wu and W. Song, *J. Mater. Chem. A*, 2013, **1**, 14198.
- 18 M. A. Lim, D. H. Kim, C. O. Park, Y. W. Lee, S. W. Han, Z. Li, R. S. Williams and I. Park, *ACS Nano*, 2011, **6**, 598.
- 19 M. T. Mayer, C. Du and D. Wang, *J. Am. Chem. Soc.*, 2012, **134**, 12406.
- 20 A. Kim, Y. Won, K. Woo, C. H. Kim and J. Moon, *ACS Nano*, 2013, **7**, 1081.
- 21 M. D. Kelzenberg, S. W. Boettcher, J. A. Petykiewicz, D. B. Turner-Evans, M. C. Putnam, E. L. Warren, J. M. Spurgeon, R. M. Briggs, N. S. Lewis and H. A. Atwater, *Nat. Mater.*, 2010, **9**, 239.
- 22 Q. Li, P. Xu, B. Zhang, H. Tsai, S. Zheng, G. Wu and H.-L. Wang, *J. Phys. Chem. C*, 2013, **117**, 13872.
- 23 X. Zhang, H. Yin, J. Wang, L. Chang, Y. Gao, W. Liu and Z. Tang, *Nanoscale*, 2013, **5**, 8392.
- 24 D. Pradhan, F. Niroui and K. T. Leung, *ACS Appl. Mater. Interfaces*, 2010, **2**, 2409.
- 25 M. Jamal, M. Hasan, A. Mathewson and K. M. Razeed, *Biosens. Bioelectron.* **2013**, **40**, 213.
- 26 Y. Zhang, Y. Liu, L. Su, Z. Zhang, D. Huo, C. Hou and Y. Lei, *Sens. Actuators, B*, 2014, **191**, 86.
- 27 M. S. Hsu, Y. L. Chen, C. Y. Lee and H. T. Chiu, *ACS Appl. Mater. Interfaces*, 2012, **4**, 5570.
- 28 P. Si, S. Ding, J. Yuan, X. W. Lou and D. H. Kim, *ACS Nano*, 2011, **5**, 7617.
- 29 L. Wang, X. Gao, L. Jin, Q. Wu, Z. Chen and X. Lin, *Sens. Actuators, B*, 2013, **176**, 9.
- 30 G. Wang, X. Lu, T. Zhai, Y. Ling, H. Wang, Y. Tong and Y. Li, *Nanoscale*, 2012, **4**, 3123.
- 31 R. Ahmad, N. Tripathy and Y. B. Hahn, *Chem. Commun.*, 2014, **50**, 1890.
- 32 B. Fang, C. Zhang, W. Zhang and G. Wang, *Electrochim. Acta*, 2009, **55**, 178.
- 33 X. Jiang, T. Herricks and Y. Xia, *Nano Lett.*, 2002, **2**, 1333.
- 34 A. Kargar, Y. Jing, S. J. Kim, C. T. Riley, X. Pan and D. Wang, *ACS Nano*, 2013, **7**, 11112.
- 35 Y. S. Kim, I. S. Hwang, S. J. Kim, C. Y. Lee and J. H. Lee, *Sens. Actuators, B*, 2008, **135**, 298.
- 36 W. Zhang, X. Wen and S. Yang, *Inorg. Chem.*, 2003, **42**, 5005.
- 37 W. Zhang, S. Ding, Z. Yang, A. Liu, Y. Qian, S. Tang and S. Yang, *J. Cryst. Growth*, 2006, **291**, 479.
- 38 W. Zhang, X. Wen, S. Yang, Y. Berta and Z. L. Wang, *Adv. Mater.*, 2003, **15**, 822.
- 39 H. Zhou and S. S. Wong, *ACS Nano*, 2008, **2**, 944.
- 40 A. I. Hochbaum, R. Fan, R. He and P. Yang, *Nano Lett.*, 2005, **5**, 457.
- 41 K. Q. Peng, J. J. Hu, Y. J. Yan, Y. Wu, H. Fang, Y. Xu, S.-T. Lee, J. Zhu, *J. Adv. Funct. Mater.*, 2006, **16**, 387.
- 42 G. Wang, Y. Wei, W. Zhang, X. Zhang, B. Fang and Z. L. Wang, *Microchim. Acta*, 2010, **168**, 87.
- 43 E. J. W. Crossland, N. Noel, V. Sivaram, T. Leijtens, J. A. Alexander-Webber and H. J. Snaith, *Nature*, 2013, **495**, 215.
- 44 A. Jain, V. Aravindan, S. Jayaraman, P. S. Kumar, R. Balasubramanian, S. Ramakrishna, S. Madhavi and M. P. Srinivasan, *Sci. Rep.* 2013, DOI:10.1038/srep03002.
- 45 Y. S. Hu, Y. G. Guo, W. Sigle, S. Hore, J. P. Balaya and J. Maier, *Nat. Mater.*, 2006, **5**, 713.
- 46 C. Kong, L. Tang, X. Zhang, S. Sun, S. Yang, X. Song and Z. Yang, *J. Mater. Chem. A*, 2014, **2**, 7306.
- 47 T. Soejima, H. Yagyu, N. Kimizuka and S. Ito, *RSC Adv.*, 2011, **1**, 187.
- 48 W. Wang, L. Zhang, S. Tong, X. Li and W. Song, *Biosens. Bioelectron.*, 2009, **25**, 708.
- 49 L. Luo, L. Zhu and Z. Wang, *Bioelectrochemistry*, 2013, **88**, 156.
- 50 J. Song, L. Xu, C. Zhou, R. Xing, Q. Dai, D. Liu and H. Song, *ACS Appl. Mater. Interfaces*, 2013, **5**, 12928.
- 51 H. Gao, F. Xiao, C. B. Ching and H. Duan, *ACS Appl. Mater. Interfaces*, 2011, **3**, 3049.
- 52 L. Kong, Z. Ren, S. Du, J. Wu and H. Fu, *Chem. Commun.*, 2014, **50**, 4921-4923.
- 53 Y. Ding, Y. Wang, L. Su, M. Bellagamba, H. Zhang and Y. Lei, *Biosens. Bioelectron.*, 2010, **26**, 542.
- 54 A. A. Ensafi, M. Jafari-Asl, N. Dorostkar, M. V. Ghiaci and J. L. G. Fierro, *J. Mater. Chem. B*, 2014, **2**, 706.
- 55 B. Fang, A. Gu, G. Wang, W. Wang, Y. Feng, C. Zhang and X. Zhang, *ACS Appl. Mater. Interfaces*, 2009, **1**, 2829.
- 56 M. Segev-Bar and H. Haick, *ACS Nano*, 2013, **7**, 8366.